Synthesis of In 2 O 3 nanocrystal chains and annealing effect on their optical properties

T. S. Ko, C. P. Chu, J. R. Chen, Y. A. Chang, T. C. Lu, H. C. Kuo, and S. C. Wang

Citation: Journal of Vacuum Science & Technology A **25**, 1038 (2007); doi: 10.1116/1.2710244
View online: http://dx.doi.org/10.1116/1.2710244
View Table of Contents: http://scitation.aip.org/content/avs/journal/jvsta/25/4?ver=pdfcov
Published by the AVS: Science & Technology of Materials, Interfaces, and Processing

Synthesis of In_2O_3 nanocrystal chains and annealing effect on their optical properties

T. S. Ko, C. P. Chu, J. R. Chen, Y. A. Chang, T. C. Lu,[a] H. C. Kuo, and S. C. Wang
Department of Photonics and Institute of Electro-Optical Engineering, National Chiao Tung University, 1001 Ta Hsueh Rd., Hsinchu 30050, Taiwan, Republic of China

(Received 26 September 2006; accepted 24 January 2007; published 2 July 2007)

The authors reported the synthesis of indium oxide nanocrystal chains on silicon substrates using gold nanoparticles as catalyst on native silicon dioxide. Scanning electron microscopy investigations showed that In_2O_3 nanocrystal chains were formed. The nanocrystal chains comprised many well shaped octahedron nanoparticles with their size ranging from 20 to 100 nm connected with each other to form a network. Both high resolution transmission electron microscopy and diffraction pattern revealed that the In_2O_3 nanocrystal chains were single crystalline grown along the [111] direction. Photoluminescence study of In_2O_3 nanocrystal chains exhibited main photoemission at 544 nm due to the recombination between electrons in localized state induced by oxygen vacancies and holes in valence band. After the annealing treatment, the main photoluminescence peak not only slightly redshifted to 558 nm but also became narrower, which was attributed to the total localized state away from the conduction band caused by less defect distribution. © *2007 American Vacuum Society.* [DOI: 10.1116/1.2710244]

I. INTRODUCTION

Indium oxide (In_2O_3) is a very important wide band gap of around 3.5 eV semiconductors and has recently attracted much interest as a material for transparent electrodes in electronic devices such as liquid crystal displays,[1] solar cells,[2] sensing material,[3] and nanowire technology.[4] In recent years, there has been increasing interest in the fabrication of In_2O_3 nanostructure because of their advantages to the understanding of novel physical properties and potential applications in nanoelectronic and optoelectronic devices. Kong and Wang obtained In_2O_3 nanobelts by evaporation of In_2O_3 powders.[5] Li *et al.* grew In_2O_3 nanowires by a thermal evaporation oxidation method with a catalyst by laser ablation.[6] Alina Magdas *et al.* grew In_2O_3 nanoarrows in thermally treated indium nitride for different times.[7] Lao *et al.* observed nanochains and nanowire networks grown by a vapor transport and condensation method.[8] Though many kinds of nanostructure of In_2O_3 were developed, the reports related to nanochain structure of In_2O_3 are still limited substantially.

In this article, we successfully synthesized In_2O_3 nanochains on silicon substrates using gold nanoparticles as catalyst on native silicon dioxide. The growth mechanism will be discussed in the following section. The structural and optical properties of In_2O_3 nanochains were analyzed in detail by scanning electron microscopy (SEM), high resolution transmission electron microscopy (HRTEM), x-ray diffraction (XRD), and photoluminescence (PL). The method of thermal annealing was also used. We investigated the effect of thermal annealing on optical properties of In_2O_3 nanochains and described the reasonable mechanism in photon emission.

[a]Electronic mail: timtclu@faculty.nctu.edu.tw

II. EXPERIMENTS

Single crystal (001) oriented silicon wafers were used as substrates. Gold nanoparticles having diameters of ~20 nm were used as catalysts; they were produced by the chemical reduction of gold chloride tetrahydrate ($HAuCl_4$) with sodium citrate, and then spread onto a silicon wafer coated with a native oxide layer using a self-assembled monolayer of 3-aminopropyltrimethoxysilane as an adhesion agent. A two-zone vacuum furnace was used to grow the nanochains. Oxygen was the carry gas and flowed through the system at rate of 30 SCCM (SCCM denotes cubic centimeter per minute at STP). During the growth process, 2 g indium powders were positioned at the upstream with the samples placed at the downstream. The source vapor was transported by the carrier gas and condensed on the substrates. The temperatures were heated to 900 °C for sources and 700 °C for samples. The typical reaction time was 6 h and the growth pressure was around 0.1 torr. The morphology and microstructure of the samples were investigated by scanning electron microscopy (JEOL, JSM 6500F) and high resolution transmission electron microscopy (JEOL, JEM 2010F, operating at 200 kV). The compositions were analyzed using energy dispersive spectrometry (EDS) attached to the SEM. Selected area electronic diffraction confirmed crystal orientation of In_2O_3 nanochains. Afterward, the samples were furnace annealed in the temperature of 700 °C for 2 h in oxygen ambient. The crystal structure analysis was performed by the XRD measurement with Cu $K\alpha$ radiation. PL spectra were measured at room temperature by means of TRIAX-320 spectrometer using a 25 mW He–Cd laser with the emission wavelength of 325 nm as the excitation source.

III. RESULTS AND DISCUSSION

In general, for one-dimensional nanostructure growth, many researches have shown that the synthesis using vapor-

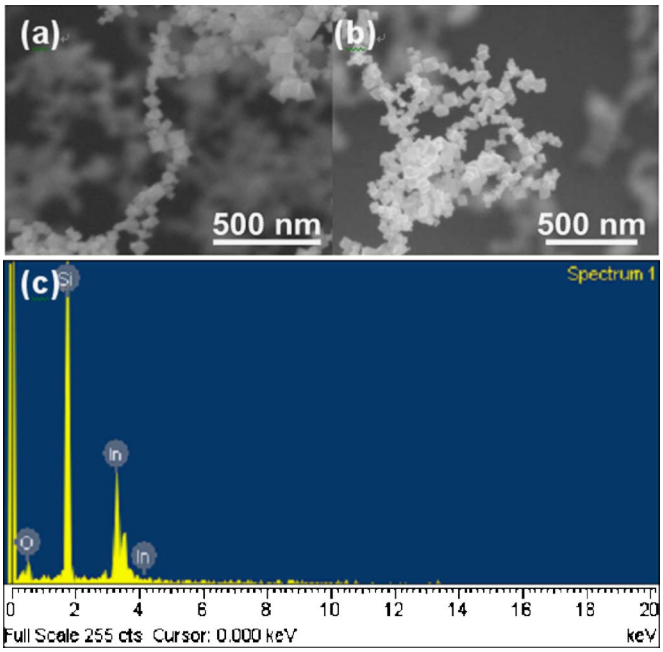

FIG. 1. [(a) and (b)] Selected area SEM images of In_2O_3 nanochains grown on a Si substrate. (c) EDS results of In_2O_3 nanochains.

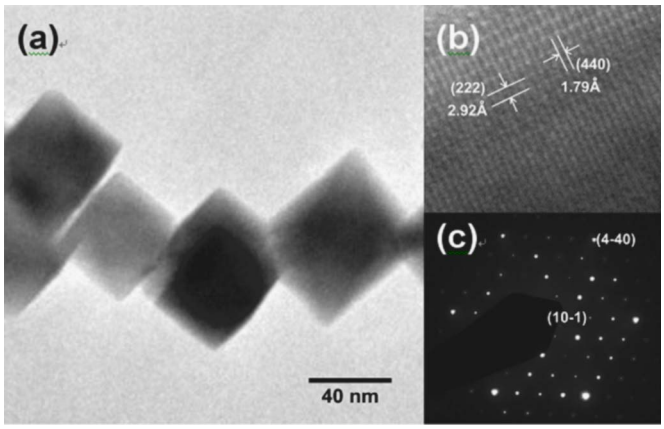

FIG. 2. (a) TEM bright-field image part of a nanochain. (b) HRTEM image of the nanochain. (c) The corresponding selected area electron diffraction pattern.

liquid-solid mechanism could obtain a constant diameter or periodically changing diameter along the growth direction without the presence of many nanocrystals with different sizes.[9–11] In contrast, we obtained very interesting self-assembled In_2O_3 nanocrystal chains with many nanoparticles of different sizes when growth pressure was 0.1 torr and temperature was 700 °C. Figures 1(a) and 1(b) show these self-assembled In_2O_3 nanochains and networks. The nanochains have diameters of between 20 and 100 nm and length of around a few micrometers. They were connected with each other to form a complicated nanonetworks. A large number of the nanoparticles of the chains would aggregate near the network junctions. Yang and Lieber grew MgO nanochains and suggested that such morphology of nanochains was grown by a vapor-solid (VS) mechanism.[12] Based on our experiment results, we found that the gold catalyst is necessary for the synthesis of the networks. However, we also observed many gold nanoparticles distributed on the substrate surface, which means the indium vapor from the upstream formed alloy with several gold nanoparticles. Meanwhile, there were also many aggregative octahedral In_2O_3 nanoparticles randomly dispersed on the substrate surface. In our growth process, therefore, the VS mechanism and gold catalyst played very important roles. We suggested it was likely that small octahedral In_2O_3 nanoparticles were formed in air and fell on the substrate at first. Consequently, the gold catalysts nucleated with the adjacent In_2O_3 nanoparticles to start nanochain growth. Once the latter indium vapor reacted with leakage oxygen near the original In_2O_3 nanoparticles/nanochains, there were more opportunities to form sequence of In_2O_3 nanoparticles and then synthesized long nanochains. We focused on different positions of In_2O_3 nanochains to proceed EDS measurement. The EDS spectrum, shown in the Fig. 1(c), indicates that the nanochains were essentially composed of indium and oxygen. The silicon peak came from silicon substrate and no gold was detected so that we suggested the gold may still remain on the substrate. Lao *et al.* grew In_2O_3 nanocrystal chains of similar shape as ours by using gold catalyst; meanwhile, they also found that there was not any gold within their nanochain structure.[8]

Figure 2(a) shows the selected TEM bright-field image of In_2O_3 nanochains. The sizes of every particle in chains were different but the shapes were uniquely octahedral shape. The junction boundary can be clearly seen between the two nanoparticles. Figure 2(b) shows the high resolution TEM image of one nanoparticle. The corresponding selected area electron diffraction (SAED) is shown in Fig. 2(c), which proved our In_2O_3 nanoparticle with chains was a single crystal structure of excellent quality. Analysis of both TEM images and SAED revealed that the In_2O_3 nanochains are single crystalline and grow along the [111] direction.

We would further study the effect of thermal annealing with oxygen at 700 °C on the structure and optical characteristics of the In_2O_3 nanochains. The XRD patterns of the In_2O_3 nanochains treated with and without thermal annealing procedures are shown in Fig. 3. The patterns correspond to In_2O_3 with the cubic structure with lattice constant of $a = 1.011$ nm (Ref. 13). Both the XRD results revealed no additional peaks corresponding to metallic indium or gold since no indium precipitates and it is difficult to detect gold monolayer. We could see the same peaks occur in both samples, which indicated the thermal annealing for the crystal orientation of the sample could not cause obvious change. The strong intensities relative to the background signal also indicated high crystallization quality of the In_2O_3 nanochains. We measured the XRD (111) rocking curves in order to compare the quality between both samples. The comparison is shown in Fig. 4. The XRD line becomes stronger and narrower as the samples are treated with thermal annealing. However, there was no clear difference in morphologies of both samples. The annealing effect could generally facilitate

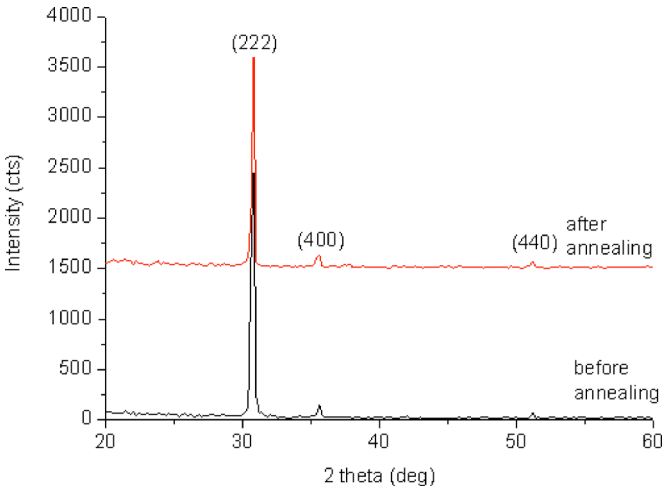

FIG. 3. XRD pattern of the In_2O_3 nanochains on Si substrate. The numbers above the peaks correspond to (*hkl*) values of the cubic structure.

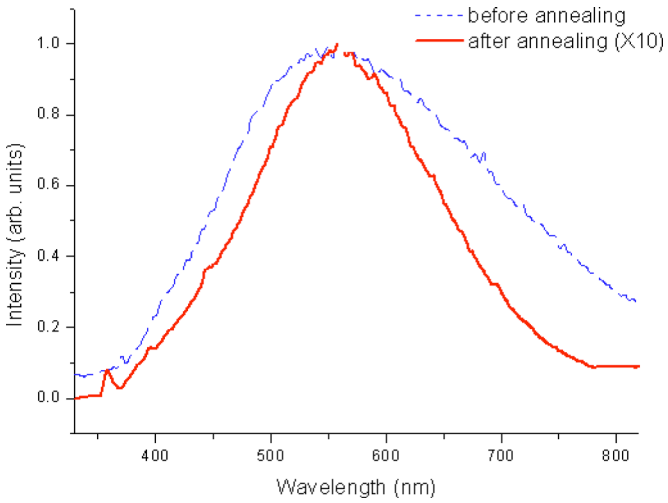

FIG. 5. Room temperature PL spectra of In_2O_3 nanochains with He–Cd laser excitation of 325 nm.

ion activation and repair defects. In other works, most defects will be pruned and the quality will be improved after annealing. Most of oxide semiconductors are native *n*-type material due to oxide vacancies.[14] Therefore, we suggested that more oxygen atoms were filled into positions of vacancies when using oxygen as carrier gas during annealing progress.

The optical properties of In_2O_3 nanochains were investigated by PL measurement. The influence of thermal annealing on optical characteristics of In_2O_3 nanochains is shown in Fig. 5. Both PL intensity curves were normalized. After thermal annealing treatment, not only the PL peaks of In_2O_3 nanochains redshifted from 544 to 558 nm but the full width of half maximal of PL spectrum also became narrower. In addition, the integrated intensity of PL emission decreased abruptly after annealing. Moreover, there was another peak occurred at 357 nm after annealing. Since In_2O_3 is a semiconductor with a band gap of around 3.6 eV (344 nm), our 544 and 558 nm PL emissions would not come from the transition of excitons from the conduction band to the valence band of In_2O_3 nanochains. On the other hand, the PL peak of 357 nm might originate from the radiative recombination of an excited carrier from the exciton state to the valence state. Many groups have studied on the optical properties of In_2O_3 compound and they have obtained different results. Liang *et al.* observed PL peaks at 470 nm from In_2O_3 nanofibers.[15] Li *et al.* measured PL of the In_2O_3 nanotubes that exhibited emission of 593 nm.[16] Lee *et al.* observed PL peak at 637 nm from In_2O_3 films.[17] The above PL mechanism was mainly attributed to the effect of the oxygen deficiencies. The reason for electronic *n*-type property of In_2O_3 is that no sufficient oxygen atoms to catch electrons released from indium atom make these electrons form the donor level. The more free electrons exist in crystal, the smaller energy gap would be between conduction band and donor level.[18] Therefore, both the PL peaks of 544 and 558 nm in our results not only revealed they were part of deep-level emission assigned to be defect-state-induced emission in In_2O_3 crystals but also indicated lower defect density caused redshift after thermal annealing, which was consistent with the results of XRD.

A schematic diagram of relative states is shown in Fig. 6. The E_L represents main localized state. The oxygen vacan-

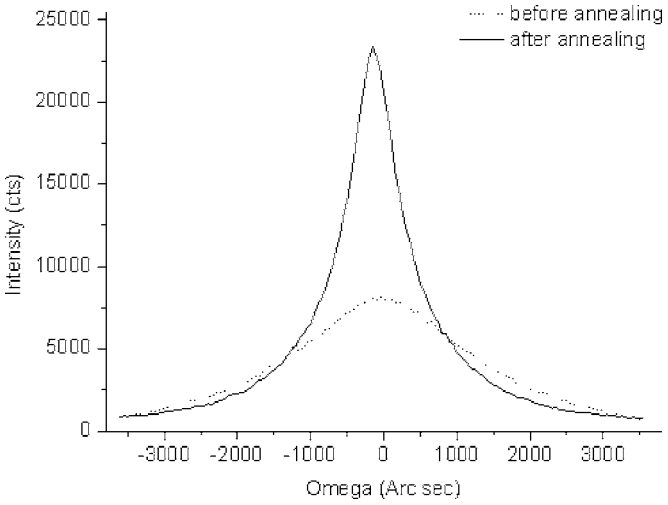

FIG. 4. XRD ω-scan data from the In_2O_3 nanochains.

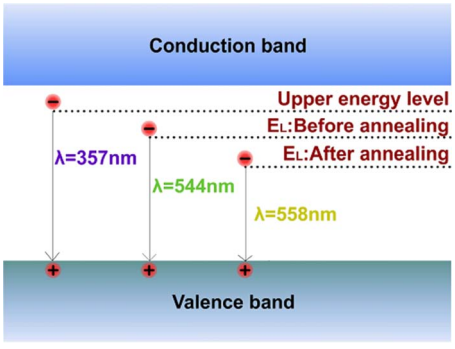

FIG. 6. Transition and emission mechanisms for In_2O_3 nanochains.

cies caused many localized states between the conduction and the valence band. The induced residual electrons in localized states would decrease after thermal annealing and exhibit a narrower linewidth in the PL spectrum. Meanwhile, the decreased numbers of electrons in the localized state produced redshift of PL peak. An electron could be excited to the upper energy level than main localized states by a pumping source and further to form an exciton. However, for oxide semiconductor materials, most native electrons from oxide deficiencies would recombine with the holes in the valence band quickly, making the exciton emission less remarkable. Therefore, once fewer electrons were in localized states after thermal annealing in our case, there could be a higher opportunity of recombination between the upper level and the valence band for the emission peak of 357 nm. As to either this energy level is an exciton state or general defect level state, further experiments still shall be done to clarify it.

IV. CONCLUSION

In conclusion, we reported the synthesis of In_2O_3 nanocrystal chains on silicon substrates using gold nanoparticles as catalyst on native silicon dioxide. The nanocrystal chains comprised many well shaped octahedron nanoparticles with their size ranging from 20 to 100 nm connected with each other to form a network. We have discussed the growth mechanism and found crystalline grown along the [111] direction by analysis of TEM. PL study pointed out main photoemission at 544 nm due to the recombination between electrons in the localized state induced by oxygen vacancies and holes in the valence band. After annealing treatment, the reduction of oxygen vacancies pushing the donor level away from the conduction band could make the main emission peak not only redshift to 558 nm but also show a narrower linewidth. Such self-assembled nanocrystal chains should have great potential for applications of novel optoelectronic devices and nanophotonics.

ACKNOWLEDGMENTS

The work was supported by the MOE ATU program and in part by the National Science Council of the Republic of China (ROC) in Taiwan under Contract Nos. NSC 95-2120-M-009-008, NSC 95-2752-E-009-007-PAE, and NSC 95-2221-E-009-282.

[1]C. Falcony, J. R. Kirtley, D. J. Dimaria, T. P. Ma, and T. C. Chen, J. Appl. Phys. **58**, 3556 (1985).
[2]C. G. Granqvist, Appl. Phys. A: Solids Surf. **57**, 19 (1993).
[3]M. Bender, N. Katsarakis, E. Gagaoudakis, E. Hourdakis, E. Douloufakis, V. Cimalla, and G. Kiriakidis, J. Appl. Phys. **90**, 5382 (2001).
[4]C. Li, D. H. Zhang, B. Lei, S. Han, X. L. Liu, and C. W. Zhou, J. Phys. Chem. B **107**, 12451 (2003).
[5]X. Y. Kong and Z. L. Wang, Solid State Commun. **128**, 1 (2003).
[6]C. Li, D. Zhang, S. Han, X. Liu, T. Tang, and C. Zhou, Adv. Mater. (Weinheim, Ger.) **15**, 143 (2003).
[7]D. Alina Magdas, A. Cremades, and J. Piqueras, Appl. Phys. Lett. **88**, 113107 (2006).
[8]J. Lao, J. Huang, D. Wang, and Z. Ren, Adv. Mater. (Weinheim, Ger.) **16**, 65 (2004).
[9]C. X. Xu, X. W. Sun, Z. L. Dong, M. B. Yu, T. D. My, X. H. Zhang, S. J. Chua, and T. J. White, Nanotechnology **15**, 839 (2004).
[10]T. Tang, S. Han, W. Jin, X. Liu, C. Li, D. Zhang, and C. Zhou, J. Mater. Res. **19**, 423 (2004).
[11]Y. Zhang *et al.*, J. Cryst. Growth **264**, 363 (2004).
[12]P. Yang and C. M. Lieber, J. Mater. Res. **12**, 2981 (1997).
[13]JCPDS Card No. 44-1087.
[14]Y. C. Kong, D. P. Yu, B. Zhang, W. Fang, and S. Q. Feng, Appl. Phys. Lett. **78**, 407 (2001).
[15]C. Liang, G. Meng, Y. Lei, F. Phillipp, and L. Zhang, Adv. Mater. (Weinheim, Ger.) **13**, 1330 (2001).
[16]Y. Li, Y. Bando, and D. Golberg, Adv. Mater. (Weinheim, Ger.) **15**, 581 (2003).
[17]M. S. Lee, W. C. Choi, E. K. Kim, C. K. Kim, and S. K. Min, Thin Solid Films **279**, 1 (1996).
[18]C. Kittel, *Introduction to Solid State Physics* (Wiley, Hoboken, NJ, 2005).